Applied Catalysis B: Environmental 94 (2010) 8–18

Contents lists available at ScienceDirect

Applied Catalysis B: Environmental

journal homepage: www.elsevier.com/locate/apcatb

Pd supported on mesoporous activated carbons with high oxidation resistance as catalysts for toluene oxidation

J. Bedia, J.M. Rosas, J. Rodríguez-Mirasol *, T. Cordero

Chemical Engineering Department, School of Industrial Engineering, University of Málaga, Campus de Teatinos s/n, 29071 Málaga, Spain

ARTICLE INFO

Article history:
Received 1 August 2009
Received in revised form 14 October 2009
Accepted 17 October 2009
Available online 29 October 2009

Keywords:
Activated carbon
Catalytic oxidation
Palladium
VOC
Toluene

ABSTRACT

Mesoporous activated carbons were obtained by chemical activation of kraft lignin with H_3PO_4 and used as supports for the preparation of carbon-based Pd catalysts with low palladium content (0.5%). The catalytic properties of the carbon-based Pd samples were evaluated in the catalytic oxidation of toluene. The effect that a thermal treatment at 900 °C in inert atmosphere carried out before and after the Pd-deposition produced on the structure and activity of the catalysts was analyzed. The catalysts obtained show high external surface areas and mesopore volumes. The chemical activation with H_3PO_4 yielded carbon supports with a significant amount of surface phosphorus, in form of C–O–PO_3, C–PO_3 and C_3PO groups. These phosphorus groups act like physical barrier, increasing the oxidation resistance of the catalysts and avoiding the burn-off of the carbon substrate during the oxidation of the VOCs. TEM analysis confirmed the presence of well-dispersed Pd particles, with sizes between 5 and 12 nm. A kinetic study of the catalytic oxidation of toluene was performed. The reaction seems to proceed through a Langmuir–Hinshelwood mechanism, whose rate-limiting step is the surface reaction between adsorbed toluene and oxygen adsorbed dissociatively, with an activation energy value of 83 kJ mol^{-1}. Toluene and xylene were oxidized to CO_2 and H_2O in the temperature range of 150–400 °C at a space velocity of 19,000 h^{-1}.

1. Introduction

The emissions of volatile organic compounds (VOCs) are generating an increasing concern due to their harmful health and environmental effects. Catalytic oxidation of VOCs to carbon dioxide and water vapor has been identified as one of the most efficient methods to eliminate these pollutants and thus to meet the increasingly stringent environmental regulations [1]. Inorganic supports, such us alumina, zeolites and metal oxides have been widely studied as catalyst supports for oxidation of VOCs [2–6]. The water vapor present in most of the gas streams and/or generated from VOCs oxidation deactivates many of the inorganic catalyst systems, which show a hydrophilic behavior. Several works have shown that the use of hydrophobic supports, as activated carbons, favors the complete oxidation of VOCs at lower temperatures [7,8]. This is a consequence of the hydrophobicity of the surface that avoids the adsorption of the water vapor molecules and therefore the deactivation of the catalyst. Besides, the hydrophobicity of the support favors the adsorption of organic compounds over the catalyst surface [9]. The acidity of the support is also known to contribute to the oxidation reaction of organic compounds [10,11].

Phosphoric acid activation is a conventional method for activated carbon preparation due to economic and environmental considerations [12,13]. This method yields carbons with acid character [14,15] and a certain cation-exchange properties similar to those of oxidized carbons [16]. The acidic compounds coming from phosphoric acid activation treatment are tightly bound to the carbon lattice as polyphosphates with C–O–P bonding [17] and are chemically and thermally more stable than those introduced by oxidative treatments. The low oxidation resistance of carbon supports is the main drawback for their use in the catalytic oxidation of VOCs. However, the presence of phosphorus compounds on the carbon surface has an inhibiting effect on the oxidation reaction at moderate temperatures [18]. Many works report the inhibition effect of organo-phosphorus compounds, H_3PO_4, $POCl_3$, acid phosphates, metal phosphates and phosphorus pentoxide. Specifically, impregnation with phosphoric acid produces C–O–P bonds that block the active carbon sites and limit the oxidation of the carbon [19,20].

Noble metals are considered suitable catalysts for the total oxidation of harmful VOCs. Palladium shows several advantages

* Corresponding author. Tel.: +34 951952385; fax: +34 951952385.
E-mail address: mirasol@uma.es (J. Rodríguez-Mirasol).

0926-3373/$ – see front matter © 2009 Elsevier B.V. All rights reserved.
doi:10.1016/j.apcatb.2009.10.015

Nomenclature

$A_{BET}^{N_2}$	apparent surface area obtained by the BET method ($m^2\ g^{-1}$)
$A_{DR}^{CO_2}$	apparent area of narrow micropores ($m^2\ g^{-1}$)
$A_t^{N_2}$	external area obtained by the t method ($m^2\ g^{-1}$)
BET	Brunauer, Emmett, and Teller
BTX	benzene, toluene and xylene
D	dispersion
d_n	average diameter (nm)
d_s	surface average diameter (nm)
d_v	volume average diameter (nm)
E_a	activation energy (kJ mol^{-1})
ER	Eley–Rideal mechanism
F_{Tol}	initial molar flow of toluene ($\mu mol\ s^{-1}$)
GHSV	gas hourly space velocity (h^{-1})
ΔH_{O_2}	adsorption enthalpy of oxygen (kJ mol^{-1})
ΔH_{Tot}	adsorption enthalpy of toluene (kJ mol^{-1})
ΔH_{ad}^0	standard enthalpy of adsorption (kJ mol^{-1})
k	reaction intrinsic kinetic constant ($mol\ g^{-1}\ s^{-1}$)
k_o	preexponential factor of Arrhenius equation ($mol\ g^{-1}\ s^{-1}$)
$K_{o_{O_2}}$	preexponential factor for oxygen adsorption (atm^{-1})
$K_{o_{Tot}}$	preexponential factor for toluene adsorption (atm^{-1})
K_{O_2}	adsorption equilibrium constant of oxygen (atm^{-1})
K_{Tol}	adsorption equilibrium constant of toluene (atm^{-1})
LH	Langmuir–Hinshelwood mechanism
M_{Pd}	palladium molar weight (106.4 g mol^{-1})
P/P_o	N_2 relative pressure
P_{Tol}	toluene inlet partial pressure (atm)
r	conversion rate of toluene ($\mu mol\ g^{-1}\ s^{-1}$)
R	universal gas constant (J $mol^{-1}\ K^{-1}$)
S_{Pd}	molar surface area of palladium ($47{,}780\ m^2\ mol^{-1}$).
ΔS_{ad}^0	standard entropy of adsorption (J $mol^{-1}\ K^{-1}$)
STP	standard temperature–pressure conditions
TEM	transmission electron microscopy
TG	thermogravimetric
TOF	turn over frequency (s^{-1})
TOS	time on stream (h)
V_{ads}	N_2 adsorbed volume (cm^3 STP g^{-1})
$V_{DR}^{CO_2}$	narrow micropore volume obtained by the DR method ($cm^3\ g^{-1}$)
$V_{mes}^{N_2}$	mesopore volume ($cm^3\ g^{-1}$)
$V_{mic}^{N_2}$	micropore volume obtained by the t method ($cm^3\ g^{-1}$)
VOC	volatile organic compound
W	weight of catalyst (g)
W/F_{Tol}	toluene space time (g s/μmol)
X	toluene conversion
X_{exp}	experimental toluene conversion
X_{calc}	simulated toluene conversion
XPS	X-ray photoelectron spectroscopy

compared to platinum, such us higher thermal stability and low cost and even higher activity depending on the organic compound [21–23]. Palladium has also been widely studied for the catalytic oxidation of methane [24–27]. The aim of this work is the preparation and characterization of Pd catalysts supported on mesoporous activated carbons with high oxidation resistance for the oxidation of toluene. The carbon supports were obtained by phosphoric acid activation of kraft lignin. Lignin is the second most abundant polymer in nature after cellulose. This natural, aromatic (phenolic), heterogeneous bio-macromolecule exists in the cell wall of plants. It is also obtained as a co-product of the papermaking industry. Furthermore, large amounts of lignins could be generated in future wood-to-ethanol bio-refineries. The development of value-added lignin-based products will be crucial to the economic success of the bio-ethanol production by this process. The presence of high stable surface phosphorus groups from the activation process provides the carbons a high oxidation resistance. The activity of the catalysts was tested for the oxidation of benzene, toluene and xylene (BTX). The effect of a thermal treatment performed before and after the deposition of Pd on the catalytic properties of the carbons was also investigated.

2. Experimental

2.1. Supports and catalysts preparation

Kraft lignin, supplied by the Empresa Nacional de Celulosas (ENCE), was obtained by acid precipitation from eucalyptus kraft black liquors. The lignin was impregnated with 85% (w/w) H_3PO_4 aqueous solution at room temperature and dried for 24 h at 60 °C in a vacuum dryer. The impregnation ratio (H_3PO_4/precursor mass ratio) used in this study was 3. The impregnated samples were activated under continuous N_2 flow (150 cm^3 STP/min) in a conventional tubular furnace. The activation temperature, 500 °C, was reached at a heating rate of 10 °C/min and maintained for 2 h. The samples were cooled inside the furnace under N_2 flow (150 cm^3 STP/min) and washed with distilled water at 60 °C until neutral pH and negative phosphate analysis in the eluate. The acid washing procedure removes almost completely the inorganic matter of the kraft lignin (as shown by XPS and thermogravimetric analyses) avoiding the catalytic effect of this inorganic matter in the subsequent VOC oxidation. The resulting activated carbons were dried at 120 °C and sieved to a particle size between 100 and 200 μm. The activated carbon obtained from kraft lignin was denoted as L. This carbon was submitted to a thermal treatment in inert atmosphere from room temperature to 900 °C at a heating rate of 10 °C/min, yielding the carbons LT.

Palladium was deposited on the different carbon supports by incipient wetting impregnation method, using aqueous solutions of palladium chloride (slightly acidified with HCl) to get a metal loading of around 0.5 wt%. After impregnation a reduction process is performed (400 °C, 3 h, N_2/H_2 = 3:1) to yield the catalysts L-Pd and LT-Pd. The effect of the thermal treatment was investigated before and after palladium impregnation. In this way, catalyst L-Pd was submitted to a thermal treatment, from room temperature to 900 °C at a heating rate of 10 °C/min, obtaining the catalysts denoted by L-PdT. Scheme 1 outlines the different treatments and the notation of the supports and catalysts obtained.

2.2. Supports and catalysts characterization

The porous structure of the samples was evaluated by N_2 adsorption–desorption at −196 °C and by CO_2 adsorption at 0 °C, carried out in an Autosorb-1 apparatus (Quantachrome). Samples were previously outgassed for at least 8 h at 150 °C. From the N_2 isotherm, the apparent surface area ($A_{BET}^{N_2}$) was determined by

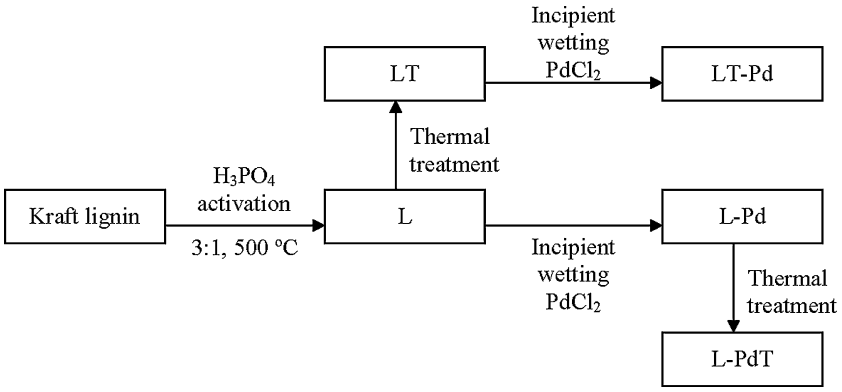

Scheme 1. Preparation procedure and notation of the supports and catalysts.

applying the BET equation. The micropore volume ($V_t^{N_2}$) and the external surface area ($A_t^{N_2}$) were obtained by applying the *t* method. The narrow mesopore volume was determined as the difference between the adsorbed volume of N_2 at a relative pressure of 0.95 and the micropore volume, $V_t^{N_2}$. From the CO_2 adsorption data, the narrow micropore volume ($V_{DR}^{CO_2}$) and the apparent surface area ($A_{DR}^{CO_2}$) were calculated using the Dubinin–Radushkevich equation.

The surface chemistry of the samples was analyzed by X-ray photoelectron spectroscopy (XPS) analyses performed using a 5700C model Physical Electronics spectrometer with Mg Kα radiation (1253.6 eV). For the analysis of the XPS peaks, the C 1s peak position was set at 284.5 eV and used as internal reference to locate the other peaks. Fitting of the XPS peaks was done by the least-squares method using Gaussian–Lorentzian peak shapes. TEM images were obtained using a PHILIPS CM-200 transmission electron microscope at an accelerating voltage of 200 kV. Particle size distributions were obtained by counting between 100 and 200 particles on each sample. The size distributions were fitted to a log normal distribution in each case. From the size distribution, we determined the following averages: the number average diameter $d_n = \sum n_i d_i / \sum n_i$, the surface average diameter $d_s = \sum n_i d_i^3 / \sum n_i d_i^2$ and the volume average diameter $d_v = \sum n_i d_i^4 / \sum n_i d_i^3$, where n_i is the number of particles with diameter d_i [28]. Palladium particle size (supposing spherical particles) and dispersion (*D*) are related by the following equation [29]:

$$d\,(\mathrm{nm}) = 6 \times 10^3 \frac{M_{Pd}}{\rho_{Pd} D S_{Pd}}$$

where M_{Pd} is palladium molar weight (106.4 g mol^{-1}), ρ_{Pd} is palladium density (12 g cm^{-3}), *D* is dispersion and S_{Pd} is molar surface area of palladium assuming an equidistribution of the low index faces (47,780 m^2 mol^{-1}).

The oxidation resistance was evaluated using a thermogravimetric analysis system (CI Electronics MK2 microbalance) under air flow (150 cm^3 STP/min), by heating the sample, of about 10 mg, from room temperature to 900 °C, at a heating rate of 10 °C/min.

2.3. Catalytic oxidation

Catalytic oxidation of benzene, toluene and xylene (mixture of isomers) was carried out in a quartz fixed bed microreactor (4 mm i.d.) at atmospheric pressure and temperatures between 150 and 425 °C. Standard experiments were performed using a catalytic bed of 150 mg of catalyst (palladium plus carbon support, 100–200 μm in size) diluted in 1 g of SiC. Silicon carbide was used to reduce gas channeling and temperature gradient in the catalytic bed and did not show any catalytic activity for the oxidation of the VOCs studied at temperature lower than 450 °C. No "in situ" reduction of the catalysts was performed prior to the VOC oxidation.

Inlet concentrations of 1000 ppm for benzene, toluene and xylene in an air flow of 100 cm^3 STP/min were used, resulting in a space time of 2.01 g s/μmol (GHSV of 19,000 m^3_{gas} h^{-1} $m^{-3}_{catalyst}$). To avoid the condensation of the reactant or any reaction product all the lines were heated above 120 °C. For the kinetic study of the toluene catalytic oxidation the most active catalyst was used, with inlet toluene concentrations between 250 and 1000 ppm and with space times from 1.08 to 4.32 g s/μmol.

The concentrations of the reactant and the VOCs oxidation products in the outlet gas stream were analyzed by gas chromatography (PerkinElmer, Autosystem GC) using an auto-sampling valve with a methyl silicone capillary column (HP-1, 50 m) and a flame ionization detector. A mass spectrometer (Omnistar^{TM}, Pfeiffer Vacuum) was used to analyze the outlet gas concentrations of CO_2, CO and H_2O. In all the cases carbon mass balances were closed with errors lower than 5%. The steady-state conversion was obtained based on VOC consumption, calculated from the inlet and outlet concentrations of VOC.

$$\mathrm{Conversion} = X = \frac{C_{inlet}^{VOC} - C_{outlet}^{VOC}}{C_{inlet}^{VOC}}$$

3. Results and discussion

3.1. Sample characterization

Fig. 1 represents the N_2 adsorption–desorption isotherms at −196 °C of the activated carbon and carbon used as supports for

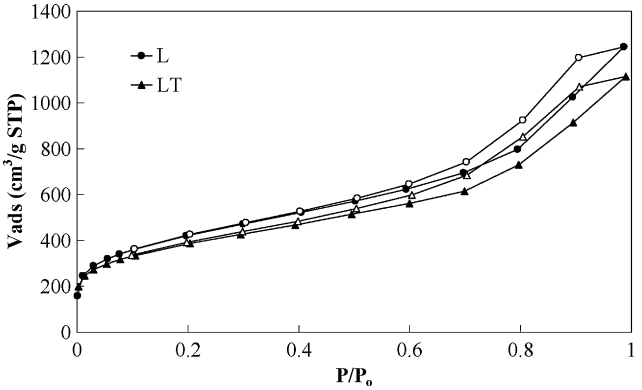

Fig. 1. N_2 adsorption–desorption isotherms at −196 °C of the carbon supports (adsorption: closed symbols; desorption: open symbols).

Table 1
Structural characteristics of the carbon supports and catalysts.

Sample	$A_{BET}^{N_2}$ ($m^2 g^{-1}$)	$V_t^{N_2}$ ($cm^3 g^{-1}$)	$A_t^{N_2}$ ($m^2 g^{-1}$)	$V_{mes}^{N_2}$ ($cm^3 g^{-1}$)	$A_{DR}^{CO_2}$ ($m^2 g^{-1}$)	$V_{DR}^{CO_2}$ ($cm^3 g^{-1}$)
L	1521	0.293	912	1.501	748	0.285
LT	1375	0.273	800	1.271	688	0.262
L-Pd	1417	0.270	858	1.360	611	0.232
LT-Pd	1248	0.220	804	1.223	601	0.229
L-PdT	1269	0.247	753	1.146	665	0.253

the preparation of the catalysts. The solids present a microporous structure with a significant contribution of mesoporosity, as indicated by the sharp increase of N_2 adsorbed volume at very low relative pressure and the presence of a large hysteresis loop, respectively. The isotherms show a round knee at low relative pressures ($P/P_o < 0.1$) suggesting the presence of a wide microporous structure. The N_2 adsorption–desorption isotherms of the Pd catalysts (not shown) are very similar to those of their corresponding carbon precursors with only a very slightly reduction of the amount of N_2 adsorbed and low relative pressures ($P/P_o < 0.1$) observed. This suggests that part of the pores is occluded by palladium particles although the reduction is not very significant, due to the low amount of Pd deposited, 0.5 wt%.

The thermal treatment carried out to the activated carbons (L) before and after Pd loading produces a solid reorganization resulting in a shrinkage of the porous structure of the carbon support [30], as indicated by the lower adsorption of N_2 observed for the heat-treated samples. The order in which the thermal treatment is applied, before or after the loading of Pd, has no effect in the porous structure of the catalysts.

The structural characteristics of the carbons, activated carbons and catalysts are reported in Table 1. This Table summarizes the apparent surface areas obtained using the BET method, the micropore volumes and external surface areas obtained using the *t* method and the mesopore volumes derived from the N_2 adsorption data. In addition, the narrow micropore surface areas, $A_{DR}^{CO_2}$, and narrow micropore volumes, $V_{DR}^{CO_2}$, obtained by the application of the DR method to the CO_2 isotherms are also included in Table 1. The carbons obtained from kraft lignin show similar values of $V_{DR}^{CO_2}$ and $V_t^{N_2}$, suggesting the presence of a homogeneous microporosity [31]. It is noteworthy the high apparent surface areas exhibited by the activated carbons and catalysts obtained, with a significant contribution of mesoporosity, very attractive for catalytic applications. L-Pd catalyst shows an $A_{BET}^{N_2}$ value of more than 1400 $m^2 g^{-1}$, with more than 800 $m^2 g^{-1}$ of external area, $A_t^{N_2}$.

The activation with phosphoric acid proceeds through the formation of phosphate and polyphosphate bridges that connect and crosslink biopolymer fragments. These phosphate groups expand the void spaces in the carbon structure producing a development of the porous structure that is released after the removal of the acid [32,33]. A high impregnation ratio, like that used in this work ($R = 3$), causes higher incorporation of phosphate esters in the solid matrix, which results in a greater expansion of the porous structure during the activation process, yielding carbons with a wider porous structure and a higher contribution of larger pores [32,33].

XPS analyses reveal the presence of C, O, N and P on the activated carbons and carbons surfaces, as well as Pd on the catalyst surfaces. Table 2 summarizes the mass surface concentration of the different samples obtained by XPS quantitative analysis. Carbon is the main component for all the samples, with surface oxygen in an amount of around 10 wt%. It is worth mentioning the significant amount of phosphorus (from about 3 to almost 6 wt%) that remains on the surface of the samples, despite the washing step carried out after the activation process. The palladium catalysts showed an amount of surface Pd close to 0.5 wt%. It is noteworthy that the thermal treatments do not decrease significantly the oxygen amount. It is necessary to take into account that XPS analyses only the carbon surface. Therefore, although the surface oxygen does not decrease significantly the total amount of oxygen decrease as shown in previous DTP analyses [20,33,34]. This is indicative of the high stability of the surface oxygen complexes formed during the phosphoric acid activation process [20,33].

Fig. 2 shows the deconvoluted P 2p spectra of the L, LT and L-Pd samples obtained from kraft lignin. The phosphorus spectra were deconvoluted using two doublet peaks with an area ratio of 0.5 and a separation between peaks of 0.84 eV [35]. The P 2p spectrum of phosphorus for L activated carbon shows a band with a main peak at a binding energy of about 133.7 eV, which is characteristic of pentavalent tetracoordinated phosphorus (PO_4) as in polyphosphates and/or phosphates [15,17,32]. Puziy et al. [17] suggested that the most probable structure for phosphorus species in polymer-based phosphoric acid activated carbons is condensed phosphates bound to carbon lattice via C–O–P bonding. This broad band may be the resulting from different peaks. A peak at a value around 134.2 eV can be assigned to P groups bonded to a carbon site throughout an O atom (C–O–PO_3 and/or $(C–O)_3PO$) [17,33,36], a second peak that appears to a binding energy of about 133.4 eV characteristic of the existence of C–P bonding as in C–PO_3 and/or C_2PO_2 [17,33,36], a small peak at around 132.1 ascribed to C_3PO groups and an almost negligible peak at 131.0 eV related to C_3P groups [35]. On the following we will refer to C–O–PO_3 and/or $(C–O)_3PO$ groups as C–O–PO_3 groups and C–PO_3 and/or C_2PO_2 as C–PO_3.

Table 2
Mass surface concentration obtained by XPS quantitative analysis.

Sample	%C 1s	%O 1s	%Pd 3d	%N 1s	%P 2p
L	84.48	11.47	–	0.35	3.70
LT	82.80	11.71	–	0.75	4.74
L-Pd	86.27	9.90	0.43	0.29	3.12
LT-Pd	84.77	9.50	0.50	0.77	4.46
L-PdT	83.45	9.44	0.52	0.62	5.99

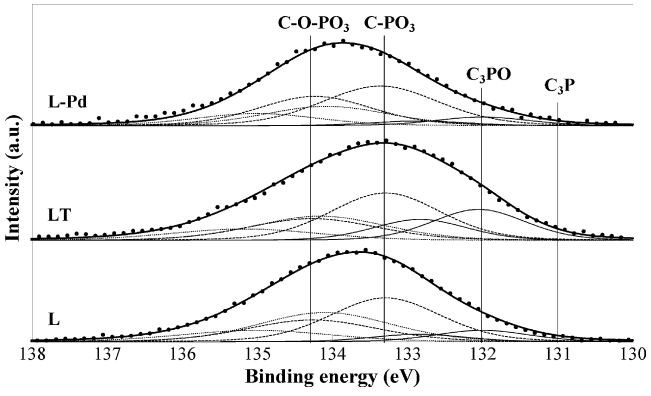

Fig. 2. P 2p deconvoluted spectra of L, LT and L-Pd samples.

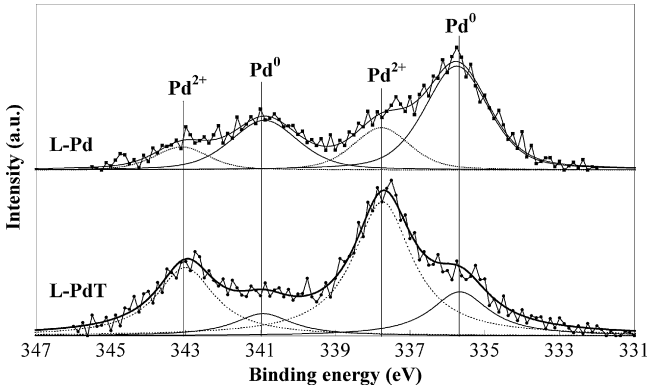

Fig. 3. Pd 3d deconvoluted spectra of L-Pd and L-PdT samples.

The thermal treatment of L carbon produced a displacement of the maximum of the P 2p spectrum signal to lower binding energies. This suggests that the carbonization process causes a decomposition of the less stable C–O–PO_3 groups, increasing the amount of C–PO_3 and C_3PO groups. The process of Pd-deposition on the lignin-derived activated carbon (L-Pd) and carbon (LT-Pd) produced an opposite behavior, shifting the P 2p spectra to higher binding energy values. A possible explanation is that the electrodeficient palladium (Pd^{2+}) is reduced to metallic palladium (Pd^0) during the treatment in H_2, oxidizing part of the surface phosphorus groups and, therefore, shifting the P 2p spectra to higher binding energy values.

The Pd region of the spectra for all the catalysts present a doublet corresponding to Pd $3d_{5/2}$ and Pd $3d_{3/2}$ [35]. The separation between Pd $3d_{3/2}$ and Pd $3d_{5/2}$ peaks, due to spin orbital splitting, is a quantized value of 5.3 eV. The Pd $3d_{5/2}$ peak lying at around 335.7 eV can be attributed to Pd^0 (metallic Pd), while the Pd $3d_{5/2}$ peak located at around 337.5 eV is related to Pd^{2+} (electrodeficient palladium) [37,38]. Fig. 3 represents the Pd 3d deconvoluted spectra for L-Pd and L-PdT catalysts. Pd on L-Pd catalyst is present mainly in form of Pd^0, with low amount of Pd^{2+}. The thermal treatment produces a shift of the peaks to higher binding energies, which suggest higher proportion of Pd in form of Pd^{2+} in the heat-treated catalyst (L-PdT). The mass percentage of surface palladium species (Pd^0 and Pd^{2+}), obtained by deconvolution of the XPS Pd 3d region spectra, is summarized in Table 3. Metallic palladium is the main chemical state of palladium (60–75 wt%) in the surface of the catalysts L-Pd and LT-Pd. This suggests that the reduction, performed to these catalysts as final treatment, yielded carbons samples with palladium mainly in form of metallic palladium, with a relatively small proportion of electrodeficient palladium. In the catalyst L-PdT, the surface palladium is mainly in form of Pd^{2+} (around 75 wt%). This seems to indicate that during the thermal treatment applied to these catalysts the metallic palladium is oxidized to Pd^{2+} by the reduction of C–O–PO_3 groups to C–PO_3 and C_3PO groups. Furthermore, CO_2 (evolved from the decomposition of the oxygen surface groups of the carbons during heating) is able to dissociate on the surface of the catalysts, yielding highly oxidative O species which could oxidize Pd^0 into Pd^{2+} [39,40].

Table 3
Mass surface proportion of Pd^0 and Pd^{2+}.

Catalyst	Pd^0 (wt%)	Pd^{2+} (wt%)
L-Pd	71.7	28.3
LT-Pd	59.8	40.2
L-PdT	22.9	77.1

The structure and the Pd distribution of the catalysts obtained from lignin (L series) were analyzed by TEM microscopy. Fig. 4a–c shows TEM images of the L-Pd, L-PdT and LT-Pd catalysts, respectively. Palladium particles, showed as darker spots, seem to be dispersed and essentially spherical. Based on the measurements of a number of particles between 100 and 200 in random regions, the corresponding histograms for L-Pd, L-PdT and LT-Pd catalysts (Fig. 4d–f, respectively) have been obtained. The particles size distributions have been fitted to a normal distribution with mean μ and standard deviation σ. Table 4 summarizes the average diameter, the standard deviation, the surface average diameter, the volume average diameter and the dispersion. In the case of L-Pd catalyst the Pd particles seem to be well dispersed with a narrow size distribution (lowest value of the standard deviation), with particles mainly between 3 and 6 nm in size and an average diameter of 4.5 nm. The high dispersion could be due to the use of $PdCl_2$ as palladium precursor [41]. Furthermore, Suh et al. [42] affirmed that the metal dispersion of carbon-supported palladium catalysts increased with the amount of surface oxygen groups. On the other hand, Cabiac et al. [43] stated that the prime parameter which determines the Pd particle size is the extent of the activated carbon surface in meso- and macropores. The high dispersion of Pd particles showed on the carbons studied in this work could be due to the high amount of oxygen surface groups and the high mesopore volume of the activated carbons produced by chemical activation with phosphoric acid [20,33,44]. In addition, Calvo et al. [45,46] asserted that the presence of a high amount of acidic groups results in a decrease in the hydrophobicity of the support, which may enhance the diffusion of the metal precursor. The activation with phosphoric acid results in carbons with high surface acidity [44] and decreases the carbon surface hydrophobicity [33], which could enhance the palladium dispersion.

The particle size distribution of the L-PdT catalyst (Fig. 4e) shows a broad distribution with a mean diameter of 11.7 nm. The thermal treatment seems to produce some sintering of the Pd particles which results in a lower dispersion and a higher particle size. This is in agreement with the results of Datye et al. [47] who conclude that the sintering of Pd at temperatures of around 900 °C occurs via interparticle transport due to the high vapor pressure of Pd at this temperature. The particle size distribution of LT-Pd catalyst (Fig. 4f) shows a mean diameter of 9.7 nm, higher than that corresponding to L-Pd catalyst and lower than that for L-PdT catalyst. The lower dispersion of LT-Pd catalyst could be due to the aforementioned effect of the surface oxygen groups [42]. The thermal treatment performed to the carbon support at 900 °C removes part of the surface oxygen groups decreasing the palladium dispersion and increasing the palladium particle size.

A key property of carbon-based catalysts for their application in oxidation reactions is their oxidation resistance. The oxidation resistance was evaluated using a thermogravimetric analysis system (TG) under air flow. Fig. 5 represents the non-isothermal oxidation resistances profiles of the supports and catalysts obtained from kraft lignin. All the samples show high oxidation resistances, with no significant oxidation at temperatures below 450 °C. It seems that the phosphorus bonded to the carbon surface increases the oxidation resistance of the carbon supports, since phosphorus is used as inhibitor of the oxidation of carbon materials [18,19]. The thermal treatment increases the oxidation resistance of the carbon support (L) and the Pd supported carbon (L-Pd). This suggests that this treatment produces a slight structural organization of the carbon matrix, with a contraction of the porous structure due to the reduction of the space between the graphene layers (Fig. 1 and Table 1) as previously reported for other carbon materials [30,48,49]. Besides, with the heat treatment the amount of surface phosphorus increases (Table 2), specially that corresponding to C-PO_3 and C_3PO groups (Fig. 2), which play a

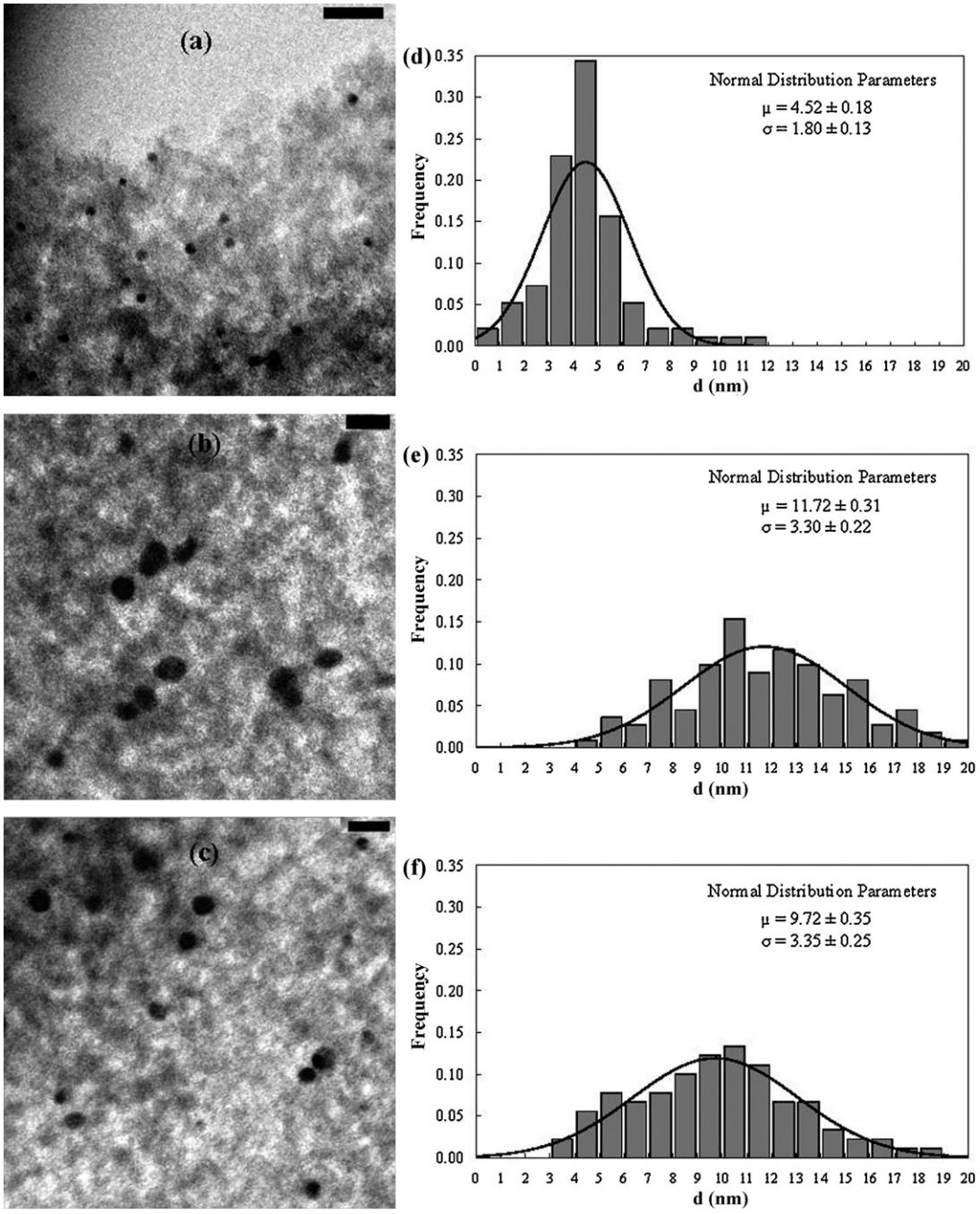

Fig. 4. TEM images (a–c) and particle size distribution histograms (d–f) of the L-Pd, L-PdT and LT-Pd catalysts, respectively (bar lengths: 30 nm).

key role in the carbon oxidation inhibition [36,20]. These P surface groups may act as physical barrier, blocking the active carbon sites for the oxidation reaction [18,19]. The impregnation with Pd decreased the oxidation resistance of the catalysts, since palladium is a known catalyst of the oxidation reaction.

Table 4
Palladium crystallite sizes from TEM, dispersion and TOF at 300 °C.

	d_n (nm)	σ	d_s (nm)	d_v (nm)	D (%)	$10^2 \times$ TOF (s^{-1})
L-Pd	4.5	1.8	6.0	6.9	24.8	0.258
L-PdT	11.7	3.3	13.5	14.2	9.6	6.138
LT-Pd	9.7	3.4	11.9	12.7	12.6	2.856

3.2. Catalytic oxidation of VOCs

Catalytic oxidation of BTX was carried out in a quartz fixed bed microreactor at atmospheric pressure. The absence of mass transfer limitations at the reaction conditions was verified theoretically. The external diffusion mass transfer resistance was evaluated by the estimation of the Damköhler number [50]. In the most unfavorable conditions, a Damköhler number of 2.10×10^{-2} was obtained, suggesting the absence of external mass transfer limitations. The influence of internal mass transfer was evaluated using the criterion of Weisz [51], according to which internal mass transfer effects can be neglected for values of the dimensionless Weisz number lower than 0.15 [51]. In our case, the

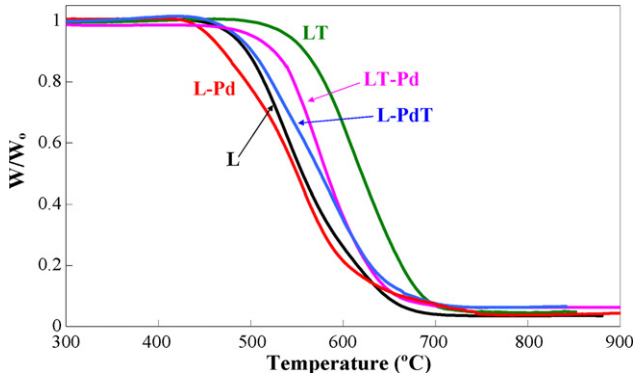

Fig. 5. TG profiles in air of supports and catalysts from kraft lignin.

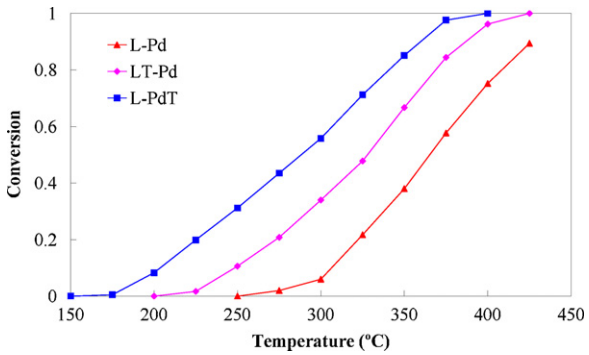

Fig. 6. Conversion of toluene (1000 ppm inlet concentration) on different catalysts as a function of the reaction temperature in air flow at a space time of 2.015 g s/μmol.

Weisz number was 2.41×10^{-2} in the most unfavorable case. Taking into account the diluted VOC concentration (<1000 ppm) and that the carbon catalysts were dispersed in SiC, it can be assumed that thermal effects are negligible.

Concerning the reactor model, according to the literature [51,52] by-pass and axial dispersion effects can be neglected for reactor diameter to particle diameter ratio higher than 10, and catalytic bed length to particle diameter ratio higher than 50. In the present work plug flow reactor can be assumed, given that the values for these ratios were 27 and 287, respectively.

The steady-state conversion of toluene (1000 ppm inlet concentration) as a function of reaction temperature for different catalysts in air flow at a space time of 2.015 g s/μmol is shown in Fig. 6. Steady-state conversion increases with the reaction temperature for all the catalysts studied. The reaction temperature was maintained below 425 °C to prevent the burn-off of the catalyst support. In all the cases, complete oxidation of toluene to CO_2 and H_2O was observed. Benzene was only observed in some cases at the higher reaction temperatures as dealkylation product, but in trace concentrations (<10 ppm). The catalyst not submitted to thermal treatment (L-Pd) showed the lowest conversions, whereas L-PdT displayed the highest conversion of all the studied catalysts. A possible explanation for this behavior is that metallic palladium, predominant in L-Pd catalyst, is less active in the catalytic oxidation of toluene than Pd^{2+} (probably as PdO), the main chemical state of palladium in L-PdT catalyst. In the literature there is no agreement about what form of palladium is more active for the oxidation reaction. Some authors state [53,54] that Pd^{2+} is more active than metallic palladium for catalytic oxidation reaction whereas other authors [55] affirm just the opposite. Other possible explanation is related to the palladium particle size. As can be seen in Table 4 the increase of dispersion strongly decreased the turn over frequency (TOF), revealing that the oxidation of toluene catalyzed by the Pd supported on the activated carbons obtained in this work was structure-sensitive. This is in agreement with the structure-sensitive behavior observed for palladium catalysts supported on alumina for methane oxidation [56,57] and on silica–alumina for aerobic oxidation of alcohols [58]. However, Papaefthimiou et al. [23] stated that the activity of palladium catalysts supported on alumina for combustion of non-halogenated volatile organic compounds was only weakly dependent on Pd particle size. The effect of the palladium particle size on the catalytic hydrocarbon reaction is highly dependent on the catalytic support and the reaction studied. Furthermore, in the case of palladium two types of PdO species are identified: bulk PdO and palladium oxide interacting with the support. The bulk PdO is characteristic of catalysts with low dispersion while the other specie is associated to high metal dispersions with low particle sizes. Each palladium specie shows a different oxygen adsorption/desorption behavior and the strength of the Pd-O bond depends on the crystallite size [59,60]. Therefore the variation of the TOF of the toluene oxidation could be related to the changes on the electronic structure of palladium with the particle size [61].

Fig. 7 represents the steady-state conversion of BTX (1000 ppm inlet concentration) on L-PdT catalyst with the reaction temperature in air flow at a space time of 2.015 g s/μmol. The activity of the catalyst with respect to the VOC molecule change according to the following sequence: xylene > toluene > benzene. There were no significant differences in the conversion values obtained for the three different xylene isomers (*o*-, *m*- and *p*-). Benzene could not be completely oxidized at the conditions used without partial oxidation of the catalyst support (at 425 °C a conversion of 0.5 is achieved), but it has to be considered that the value of the GHSV used in this work (19,000 h^{-1}) is relatively high if it is compared with other studies of oxidation of VOCs over catalysts supported on activated carbons [7,8,62] and also higher than the reported by Morales-Torres et al. [63], although these authors used monolithic supports with palladium and platinum catalysts. At lower GHSV values higher benzene conversions could be achieved. The behavior of a catalytic system is strongly dependent on the combination of the catalyst properties and the physicochemical characteristics of the VOCs molecules, such us strength of adsorption, ionization potential and the strength of the VOC weakest C–H bond [64–66]. In this sense, in the case of Pd catalysts Becker and Föster [67] reported that xylene and toluene were more reactive reactants because of the lower ionization potentials of the methyl derivates. The ionization potentials of benzene and its methyl derivates are 9.24 eV for benzene, 8.82 eV for toluene and 8.56 eV for xylene, therefore benzene would be the most difficult to oxidize. This agrees fairly well with the results obtained in this work. Benzene and xylene are oxidized to CO_2 and H_2O. In the case

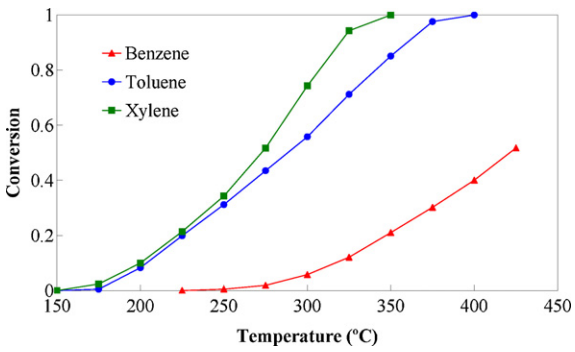

Fig. 7. Conversion of BTX (inlet concentration 1000 ppm) with the reaction temperature on L-PdT catalyst in air flow at a space time of 2.015 g s/μmol.

of the oxidation reaction of xylene at high reaction temperatures traces of toluene (<2 ppm) and benzene (<6 ppm) were observed.

TOFs of 1.1×10^{-2} and 9.1×10^{-3} s^{-1} were obtained for the oxidation of xylene and toluene at 200 °C and a value of 6.4×10^{-3} s^{-1} was calculated for benzene at 300 °C. These values are significantly higher than those reported by Morales-Torres et al. [63] for the oxidation of *m*-xylene and toluene (5.6×10^{-4} and 6.2×10^{-4} s^{-1}, respectively) at a slightly lower temperature of 160 °C. Furthermore, these authors used lower GHSV values for a monolithic support (2000 h^{-1} versus 19,000 h^{-1} in our work) and even though the catalysts were supported on carbon nanofibers coated in the monoliths, with a preparation procedure much more complex and expensive than that used for the preparation of the palladium supported activated carbons obtained by a simple incipient wetting on carbons obtained from industrial by-products. The TOF value of benzene oxidation is significantly higher than the obtained for palladium supported on vanadium oxide/alumina catalysts [61]. It has to be pointed that Ferreira et al. [61] reported the TOF value at lower temperature (177 °C) and higher space velocity (30,000 h^{-1}), although again with a more complex catalysts and with a higher amount of palladium (0.8–0.9 wt%). Therefore, the activity of L-PdT carbon for the catalytic oxidation of BTX compares quite well with the results reported in the literature with the advantage that it is obtained from an industrial by-product, by a simple preparation procedure and with low palladium content (0.5%), which make it very attractive from an economical point of view.

The stability of the carbon catalysts in oxidation reactions is a critical factor because of carbon burn-off in this atmosphere. Fig. 8 represents the toluene conversion (inlet concentration 1000 ppm) on L-PdT catalyst as a function of time on stream (TOS) at 350 °C in air flow at a space time of 2.015 g s/μmol. The catalyst was quite stable for 30 h, with no significant changes in the conversion or selectivity (complete oxidation to CO_2 and H_2O, with only traces of benzene) during the extent of the experiment. The weight of the catalyst bed showed no significant change after the reaction, confirming that the carbon support was not oxidized.

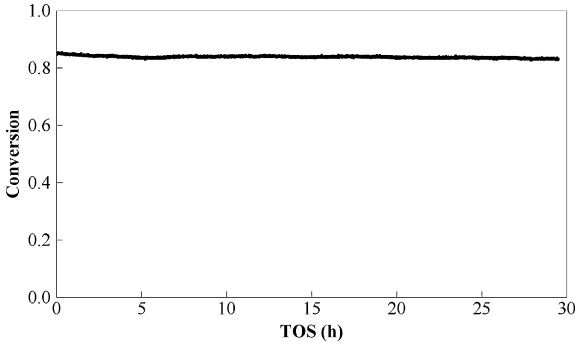

Fig. 8. Toluene conversion (inlet concentration 1000 ppm) as a function of (TOS) at 350 °C on L-PdT catalyst in air flow at a space time of 2.015 g s/μmol.

3.3. Kinetic modelling

The kinetic study was performed on the carbon catalyst with the highest activity, L-PdT, for the catalytic oxidation of toluene. Inlet toluene concentration was varied between 250 and 1000 ppm ($2.5 \times 10^{-4} < P_{Tol} < 1.0 \times 10^{-3}$ atm) and space time between 1.081 and 4.325 g s/μmol. Catalytic oxidation temperatures were on the range of 250–400 °C. Fig. 9a–c displays the experimental steady-state toluene conversions (symbols) as a function of space time at different reaction temperatures and at inlet toluene partial pressures of 2.5×10^{-4}, 5.0×10^{-4} and 1.0×10^{-3} atm, respectively. Toluene conversion increases with space times and reaction

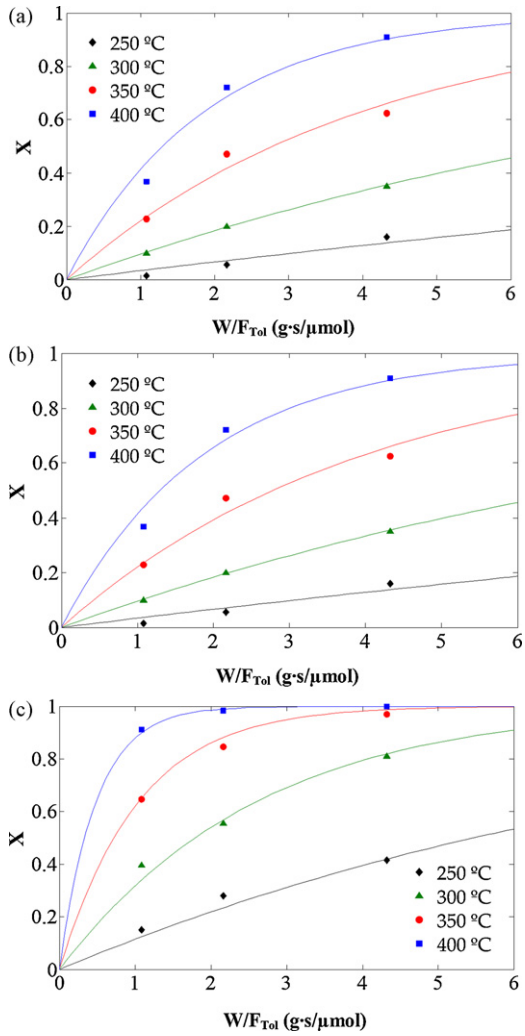

Fig. 9. Toluene conversion on L-PdT catalyst versus space time at different reaction temperatures and at inlet toluene partial pressures of (a) 2.5×10^{-4}, (b) 5.0×10^{-4} and (c) 1.0×10^{-3} atm (symbols, experimental values and solid lines, model fitting).

temperature in all the cases. Fig. 10a–c represents the experimental steady-state toluene conversions (symbols) versus inlet toluene partial pressure at different temperatures and at space times of 1.081, 2.162 and 4.325 g s/μmol, respectively. Toluene conversion increases with the toluene inlet partial pressure at the conditions analyzed.

Integral reactor behavior was used for the interpretation of the experimental data. To this purpose the reactor continuity Eq. (1) was integrated numerically to calculate the exit conversion of the toluene oxidation reaction.

$$\frac{dX}{d(W/F_{Tol})} = r \quad (1)$$

In Eq. (1), r represents the conversion rate of toluene, X is the total conversion of toluene, and (W/F_{Tol}) is the toluene space time. The following assumptions were considered: homogeneous distribution of active sites on the catalyst surface, the catalyst was operated at steady-state conditions and diffusional constraints, transport limitations and changes in temperature and pressure within the reactor were neglected. CO_2 and H_2O were the only reaction products of the oxidation reaction of toluene, given that only traces of benzene (<10 ppm) were obtained by dealkylation of toluene.

Several kinetics models were proposed to describe the kinetic of the catalytic oxidation of toluene over L-PdT catalyst. The

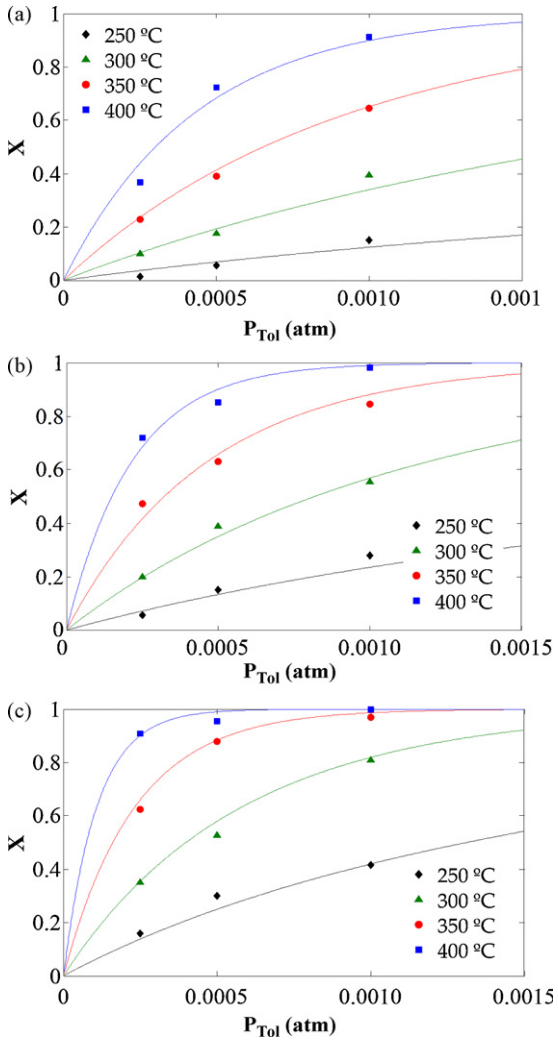

Fig. 10. Toluene conversion versus inlet toluene partial pressure at different temperatures and at space times of (a) 1.081, (b) 2.162 and (c) 4.325 g s/μmol (solid lines, model fitting and symbols, experimental values).

controlling step of the proposed models could be the surface reaction between two adsorbed molecules, Langmuir–Hinshelwood mechanism (LH), or between an adsorbed molecule and a molecule in gas phase, Eley–Rideal mechanism (ER). Table 5 summarizes the rate expressions for the proposed mechanisms analyzed in this work for toluene oxidation on L-PdT catalyst with their respective rate-limiting steps. Mars van Krevelen mechanism, often used in the literature for catalytic oxidation reactions, has been disregarded on the basis of a work of Vannice [68] who stated that the rate expression derived from this mechanism has no physical relevance and must be considered only as a mathematical fitting function. The dependence of the kinetic constant with the temperature was considered to follow an Arrhenius law (Eq. (2)). The adsorption constants follow a Van't Hoff law (Eqs. (3) and (4)).

$$k = k_o \exp\left(\frac{-E_a}{RT}\right) \tag{2}$$

$$K_{Tol} = K_{o_{Tol}} \exp\left(\frac{-\Delta H_{Tol}}{RT}\right) \tag{3}$$

$$K_{O_2} = K_{o_{O_2}} \exp\left(\frac{-\Delta H_{O_2}}{RT}\right) \tag{4}$$

k_o, $K_{o_{Tot}}$ and $K_{o_{O_2}}$ represent the respective preexponential factors, E_a the activation energy and ΔH_{Tot} and ΔH_{O_2} the adsorption enthalpies of toluene and oxygen, respectively.

The parameters were estimated by the Runge–Kutta method minimizing the error function:

$$\text{error} = \sum_i (X_{exp,i} - X_{calc,i})^2 \tag{5}$$

where X_{exp} is the value of the conversion of each reaction obtained experimentally and X_{calc} is the simulated value. The optimization routine was based in the Levenberg–Marquardt algorithm. Those mechanisms which led to thermodynamically inconsistent adsorption heats or activation energies or to negative kinetic parameters were rejected. In these conditions, the model with the best fit and the lowest error value was LH2 model, whose rate-limiting step is the surface reaction between adsorbed toluene and dissociative adsorbed oxygen. LH1 model, whose rate-limiting step is the surface reaction between adsorbed toluene and molecular adsorbed oxygen fits also relatively well the experimental data, although with a higher error value than that obtained for LH2 model. None of the models based on Eley–Rideal mechanisms reproduced the experimental results. Fig. 11 represents the values of the calculated conversion by LH2 model versus the conversion obtained experimentally. The model fits accurately the experimental data. The quality of the fitting is also observed in Figs. 9 and 10, in which the model fitting (solid lines) are represented in addition to the experimental values (symbols).

Table 6 summarizes the values of the preexponential factors, activation energy and adsorption enthalpies obtained from numerical fitting of the experimental data to LH2 model. The obtained enthalpies of adsorption (ΔH_{Tot} and ΔH_{O_2}) are negative, in agreement with an exothermic process. The standard entropy in gas phase values, S_g^0, for toluene and oxygen are 320.7 [69] and 205.2 J mol^{-1} K^{-1} [70], respectively. The standard enthalpy and entropy of adsorption are related by the expression:

$$\text{Ln}\,(K) = \frac{-\Delta H_{ad}^0}{RT} + \frac{\Delta S_{ad}^0}{R} \tag{6}$$

Table 5
Rate expressions for the proposed mechanisms for toluene oxidation on L-PdT catalyst.

Model	Rate-limiting step	Rate expression
LH1	Surface reaction between adsorbed toluene and adsorbed molecular oxygen	$-r = \frac{k_r K_{Tol} K_{O_2} P_{Tol} P_{O_2}}{(1+K_{Tol}P_{Tol}+K_{O_2}P_{O_2})^2}$
LH2	Surface reaction between adsorbed toluene and dissociative adsorbed oxygen	$-r = \frac{k_r K_{Tol} P_{Tol} \sqrt{K_{O_2} P_{O_2}}}{(1+K_{Tol}P_{Tol}+\sqrt{K_{O_2}P_{O_2}})^2}$
ER1	Surface reaction between adsorbed toluene and molecular oxygen in gas phase	$-r = \frac{k_r K_{Tol} P_{Tol} P_{O_2}}{1+K_{Tol}P_{Tol}}$
ER2	Surface reaction between toluene in gas phase and adsorbed molecular oxygen	$-r = \frac{k_r K_{O_2} P_{Tol} P_{O_2}}{1+K_{O_2}P_{O_2}}$
ER3	Surface reaction between toluene in gas phase and dissociative adsorbed oxygen	$-r = \frac{k_r P_{Tol} \sqrt{K_{O_2} P_{O_2}}}{1+\sqrt{K_{O_2}P_{O_2}}}$

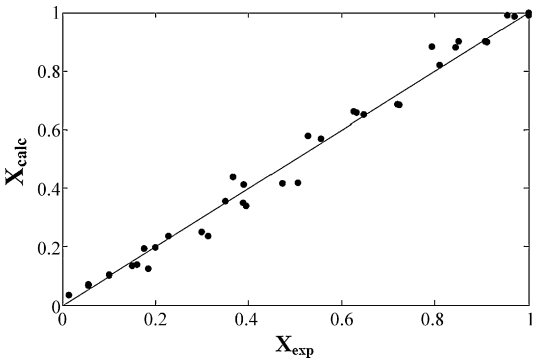

Fig. 11. Calculated conversion versus experimental conversion for LH2 model.

Table 6
Parameter values for the LH2 model.

k_o (mol g^{-1} s^{-1})	E_a (kJ mol^{-1})	$K_{o_{Tot}}$ (atm^{-1})	ΔH_{Tot} (kJ mol^{-1})	$K_{o_{O_2}}$ (atm^{-1})	ΔH_{O_2} (kJ mol^{-1})
5.50×10^8	82.86	1.77×10^{-14}	−271.20	1.69×10^{-9}	−168.51

The values of ΔS^0_{ad} for toluene and oxygen are −263.1 and −167.8 J mol^{-1} K^{-1}, respectively. Therefore, the standard entropy of adsorption, ΔS^0_{ad}, is negative and presents an absolute value smaller than that for S^0_g [71,72]. The value of the activation energy, 83 kJ mol^{-1}, is between the 75 kJ mol^{-1} obtained by Radic et al. [73] and the 106 kJ mol^{-1} calculated by Ordóñez et al. [74] for the catalytic oxidation of toluene on Pt/Al_2O_3 catalyst using a Mars van Krevelen model with non-equilibrium dissociative adsorption of oxygen on the catalyst surface. It is also similar to the apparent activation energy of 92 kJ mol^{-1} obtained by Papaefthimiou et al. [23] for the catalytic oxidation of benzene on a Pd/Al_2O_3 catalyst using a power law rate equation. The value is significantly lower than the apparent activation energies of 161 and 116 kJ mol^{-1} reported by Morales-Torres et al. [63] for the oxidation of toluene on palladium catalysts supported on monoliths with and without carbon nanofibers, respectively, using also a power law rate equation.

4. Conclusions

Carbons obtained by chemical activation of kraft lignin with H_3PO_4 were used as supports for the preparation of carbon-based Pd catalysts. The activation process yielded carbons with a wide porous structure and a high contribution of mesoporosity, which make the carbons very suitable for catalytic applications. A significant amount of phosphorus remained over the carbon surface in form of C–O–P, C–P–O and C_3PO groups, despite the washing process performed after the activation step. These groups seem to act like a physical barrier, inhibiting the oxidation of the catalyst support during the oxidation of the VOCs.

The amount of palladium on the carbon surface is about 0.5 wt%. Metallic palladium is the main chemical state of palladium in the surface of C-Pd, CT-Pd, L-Pd and LT-Pd catalysts, as a consequence of the final reduction treatment performed to these catalysts. On the other hand, in C-PdT and L-PdT catalysts, the surface palladium is mainly in form of electrodeficient palladium (Pd^{2+}), indicating that during the final thermal treatment applied to these catalysts, the metallic palladium is oxidized to electrodeficient palladium, probably, by the CO_2 desorbed from the carbon surface during the thermal treatment. TEM micrographs showed Pd nanoparticles well dispersed with a homogeneous size of about 5–12 nm, although the thermal treatment produced a clustering of the palladium particles, decreasing the dispersion and increasing the particle size

The activity of the catalyst was evaluated by oxidation of BTX. L-PdT catalyst shows the highest activity, probably as a consequence of the changes on the electronic structure of palladium with the particle size. The activity of the catalyst with respect to the VOC molecule change according to the following sequence: xylene > toluene > benzene. A kinetic study of the catalytic oxidation of toluene was performed, revealing that the reaction seems to proceed through a Langmuir–Hinshelwood mechanism, whose rate-limiting step is the surface reaction between adsorbed toluene and dissociative adsorbed oxygen, with an activation energy of 83 kJ mol^{-1}.

Acknowledgements

The authors thank the Ministry of Science and Innovation of Spain for financial support (DGICYT, Projects CTQ2006/11322 and NAN2004-09312-C03-03). J.B. acknowledges the assistance of the Ministry of Science and Innovation of Spain for the award of FPI grant.

References

[1] J.J. Spivey, Ind. Eng. Chem. Res. 26 (1987) 2165–2180.
[2] P. Papaefthimiou, T. Ioannides, X.E. Verykios, Appl. Catal. B: Environ. 15 (1998) 75–92.
[3] N. Burgos, M. Paulis, M.M. Antxustegi, M. Montes, Appl. Catal. B: Environ. 38 (2002) 251–258.
[4] D. Delimaris, T. Ioannides, Appl. Catal. B: Environ. 89 (2009) 295–302.
[5] S.M. Saqer, D.I. Kondarides, X.E. Verykios, Top. Catal. 52 (2009) 517–527.
[6] E.M. Cordi, J.L. Falconer, J. Catal. 162 (1996) 104–117.
[7] K.T. Chuang, B. Zhou, S. Tong, Ind. Eng. Chem. Res. 33 (1994) 1680–1686.
[8] R.K. Sharma, B. Zhou, S. Tong, K.T. Chuang, Ind. Eng. Chem. Res. 34 (1995) 4310–4317.
[9] J.C.S. Wu, T.Y. Chang, Catal. Today 44 (1998) 111–118.
[10] A. Ishikawa, S. Komai, A. Satsuma, T. Hattori, Y. Murakami, Appl. Catal. A 110 (1994) 61–66.
[11] F.J. Maldonado-Hódar, L.M. Madeira, M.F. Portela, R.M. Martín-Aranda, F. Freire, J. Mol. Catal. A 111 (1996) 313–323.
[12] R.C. Bansal, J.B. Donnet, H.F. Stoeckli, Active Carbon, Marcel Dekker, New York, 1988.
[13] F. Rodríguez-Reinoso, in: J.W. de Patrick (Ed.), Porosity in Carbons: Characterization and Applications, Edward Arnold, London, 1995.
[14] A.M. Puziy, O.I. Poddubnaya, A. Martínez-Alonso, F. Suárez-García, J.M.D. Tascón, Carbon 40 (2002) 1493–1505.
[15] A.M. Puziy, O.I. Poddubnaya, A. Martínez-Alonso, F. Suárez-García, J.M.D. Tascón, Carbon 43 (2005) 2857–2868.
[16] Y.F. Jia, K.M. Thomas, Langmuir 16 (2000) 1114–1122.
[17] A.M. Puziy, O.I. Poddubnaya, A.M. Ziatdinov, Appl. Surf. Sci. 252 (2006) 8036–8038.
[18] D.W. McKee, in: P.A. Thrower (Ed.), Oxidation Protection of Carbon Materials, Marcel Dekker, New York, 1991, pp. 173–232.
[19] S. Labruquère, P. Pailler, R. Naslain, B. Desbat, J. Eur. Ceram. Soc. 18 (1998) 1953–1960.
[20] J.M. Rosas, J. Bedia, J. Rodríguez-Mirasol, T. Cordero, Fuel 88 (2009) 19–26.
[21] K. Bendahou, L. Cherif, S. Siffert, H.L. Tidahy, H. Benaïssa, A. Aboukaïs, Appl. Catal. A. Gen. 351 (2008) 82–87.
[22] J.R. González-Velasco, A. Aranzabal, R. López-Fonseca, R. Ferret, J.A. González-Marcos, Appl. Catal. B: Environ. 24 (2000) 33–43.
[23] P. Papaefthimiou, T. Ioannides, X.E. Verykios, Appl. Catal. B: Environ. 13 (1997) 175–184.
[24] D. Ciuparu, L. Pfefferle, Catal. Today 77 (2002) 167–179.
[25] D. Ciuparu, N. Katsikis, L. Pfefferle, Appl. Catal. A: Gen. 216 (2001) 209–215.
[26] P. Gélin, M. Primet, Appl. Catal. B: Environ. 39 (2002) 1–37.
[27] L.S. Escandón, S. Ordóñez, A. Vega, F.V. Díez, Chemosphere 58 (2005) 9–17.
[28] M.A. Vannice, Kinetics of Catalytic Reactions, Springer, New York, USA, 2005, p. 20.
[29] D. Duprez, J. Chim. Phys. 80 (1983) 487.
[30] I. Martin-Gullon, J.P. Marco-Lozar, D. Cazorla-Amoros, A. Linares-Solano, Carbon 42 (2004) 1339–1343.
[31] J. Rodríguez-Mirasol, T. Cordero, J.J. Rodríguez, Energy Fuels 7 (1993) 133–138.
[32] M. Jagtoyen, F. Derbyshire, Carbon 36 (1998) 1085–1097.
[33] J.M. Rosas, J. Bedia, J. Rodríguez-Mirasol, T. Cordero, Ind. Eng. Chem. Res. 47 (2008) 1288–1296.
[34] E. Gonzalez-Serrano, T. Cordero, J. Rodriguez-Mirasol, L. Cotoruelo, J.J. Rodriguez, Water Res. 38 (2004) 3043–3050.

[35] J.F. Moulder, W.F. Stickle, P.E. Sobol, K.D. Bomben, in: J. Chastain, R.C. King, Jr. (Eds.), Handbook of X-ray Photoelectron Spectroscopy, Physical Electronics, Inc., Eden Prairie, MN, 1995.
[36] X. Wu, L.R. Radovic, Carbon 44 (2006) 141–151.
[37] Z.M. de Pedro, L.M. Gómez-Sainero, E. González-Serrano, J.J. Rodríguez, Ind. Eng. Chem. Res. 45 (2006) 7760–7766.
[38] V.Z. Radkevich, T.L. Senko, K. Wilson, L.M. Grishenko, A.N. Zaderko, V.Y. Diyuk, Appl. Catal. A 335 (2008) 241–251.
[39] F. Dury, E.M. Gaigneaux, P. Ruiz, Appl. Catal. A 242 (2003) 187.
[40] O. Demoulin, M. Navez, J.-L. Mugabo, P. Ruiz, Appl. Catal. B: Environ. 70 (2007) 284–293.
[41] E. Díaz, A.F. Mohedano, L. Calvo, M.A. Gilarranz, J.A. Casas, J.J. Rodríguez, Chem. Eng. J. 131 (2007) 65–71.
[42] D.J. Suh, T.-J. Park, S.-K. Ihm, Carbon 31 (1993) 427–435.
[43] A. Cabiac, T. Cacciaguerra, P. Trens, R. Durand, G. Delahay, A. Medevielle, D. Plée, B. Coq, Appl. Catal. A: Gen. 340 (2008) 229–235.
[44] J. Bedia, J.M. Rosas, J. Márquez, J. Rodríguez-Mirasol, T. Cordero, Carbon 47 (2009) 286–294.
[45] L. Calvo, A.F. Mohedano, J.A. Casas, M.A. Gilarranz, J.J. Rodríguez, Carbon 42 (2004) 1377–1381.
[46] L. Calvo, M.A. Gilarranz, J.A. Casas, A.F. Mohedano, J.J. Rodríguez, Ind. Eng. Chem. Res. 44 (2005) 6661–6667.
[47] A.K. Datye, Q. Xu, K.C. Kharas, J.M. McCarty, Catal. Today 111 (2006) 59–67.
[48] J. Rodríguez-Mirasol, P.A. Thrower, L.R. Radovic, Carbon 33 (1995) 545–554.
[49] J. Rodríguez-Mirasol, T. Cordero, J.J. Rodríguez, Carbon 34 (1996) 43–52.
[50] J.J. Carberry, in: J.R. Anderson, M. Boudart (Eds.), Physicochemical Aspects of Mass Transfer and Heat Transfer in Heterogeneous Catalysis, Springer-Verlag, Berlin, 1987.
[51] O. Levespiel, Chemical Reactor Engineering: An Introduction to the Design of Chemical Reactors, third ed., Wiley, New York, 1998.
[52] D.E. Mears, Ind. Eng. Chem. Proc. Des. Dev. 10 (1971) 541–547.
[53] Y. Yazawa, H. Yoshida, N. Takagi, S. Komai, A. Satsuma, T. Hattori, Appl. Catal. B 19 (1998) 261–266.
[54] R. Burch, P.K. Loader, F.J. Urbano, Catal. Today 27 (1996) 243–248.
[55] S.C. Kim, S.W. Nahm, W.G. Shim, J.W. Lee, H. Moon, J. Hazard. Mater. 141 (2007) 305–314.
[56] R.H. Hicks, H. Qi, M.L. Young, R.G. Lee, J. Catal. 122 (1990) 280–294.
[57] P. Briot, M. Primet, Appl. Catal. 68 (1991) 301–314.
[58] J. Chen, Q. Zhang, Y. Wang, H. Wana, Adv. Synth. Catal. 350 (2008) 453–464.
[59] K. Fujimoto, F.H. Ribeiro, M. Avalos-Borja, E. Iglesia, J. Catal. 179 (1998) 431.
[60] P. Chou, M.A. Vannice, J. Catal. 105 (1987) 342.
[61] R.S.G. Ferreira, P.G.P. de Oliveira, F.B. Noronha, Appl. Catal. B 50 (2004) 243–249.
[62] M.A. Alvarez-Merino, M.F. Ribeiro, J.M. Silva, F. Carraco-Marín, F.J. Maldonado-Hódar, Environ. Sci. Technol. 38 (2004) 4664–4670.
[63] S. Morales-Torres, A.F. Perez-Cadenas, F. Kapteijn, F. Carrasco-Marín, F.J. Maldonado-Hódar, J.A. Moulijn, Appl. Catal. B 89 (2009) 411–419.
[64] S.C. Kim, J. Hazard. Mater. B91 (2002) 285–299.
[65] J.C.S. Wu, Z.A. Lin, F.M. Tsai, J.W. Pan, Catal. Today 63 (2000) 419–426.
[66] A.A. Baresi, G. Baldi, Ind. Eng. Chem. Res. 33 (1994) 2964–2974.
[67] L. Becker, H. Föster, Appl. Catal. B 17 (1998) 43–49.
[68] M.A. Vannice, Catal. Today 123 (2007) 18–22.
[69] J.A. Deon, Lange's Handbook of Chemistry, 15th ed., McGraw-Hill, New York, 1999, p. 6.46.
[70] D.R. Lide, Handbook of Chemistry and Physics, 84th ed., CRC, New York, 2004, pp. 5–23.
[71] M. Boudart, D.E. Meras, M.A. Vannice, Ind. Chem. Belg. 32 (1967) 281–284.
[72] M.A. Vannice, S.H. Hyun, B. Kalpalci, W.C. Liauh, J. Catal. 56 (1979) 358–362.
[73] N. Radic, B. Grbic, A. Terlecki-Baricevic, Appl. Catal. B 50 (2004) 153–159.
[74] S. Ordóñez, L. Bello, H. Sastre, R. Rosal, F.V. Díez, Appl. Catal. B 38 (2002) 139–149.